Generating entangled states from coherent states in circuit-QED

Shi-fan Qi[1] and Jun Jing[1, *]

[1]*School of Physics, Zhejiang University, Hangzhou 310027, Zhejiang, China*

(Dated: January 2, 2023)

Generating entangled states is self-evidently important to a wide range of applications in quantum communication and quantum information processing. Here we propose an efficient and convenient two-step protocol for generating Bell states and NOON states of two microwave resonators, merely from their coherent states. In particular, we derive an effective Hamiltonian for resonators when coupling to a superconducting Λ-type qutrit in the dispersive regime. The shift of the qutrit transition frequency is found to be dependent on the excitation number of resonators. The Hamiltonian then enables one to use carefully tailored microwave drive signals to individually control the amplitudes of two qutrit transitions associated with particular Fock states of the relevant resonators. Thereby an arbitrary desired entangled state can be generated by a typical evolution-and-measurement procedure from product coherent states. We also analysis the robustness of our protocol against the systematic error from the microwave driving intensity, the quantum dissipation of all components, and the crosstalk of two resonators. In addition, we demonstrate that our protocol can be extended to a similar scenario with a Ξ-type qutrit.

I. INTRODUCTION

Entangled states [1] of harmonic oscillators (e.g., microwave resonators) play a key role in quantum technologies, such as quantum communication [2] and quantum information processing [3]. Creation, manipulation and measuring of the entangled states in both experimental platforms [4–8] and theoretical protocols have therefore been intensively pursued for a long time [5, 9–15] and are still under an active investigation.

The simplest and yet the most popular maximally entangled states in the Fock space of the resonators are Bell states, i.e., $(|00\rangle \pm |11\rangle)/\sqrt{2}$ and $(|10\rangle \pm |01\rangle)/\sqrt{2}$, where $|0\rangle$ and $|1\rangle$ are the ground and the first excited states, respectively. Generating Bell states in photonic systems is fundamental to both quantum cryptography [16] and quantum teleportation [17]. Another widely applied entangled states are the NOON states $(|N0\rangle \pm |0N\rangle)/\sqrt{2}$ with N integer, which consist of two orthogonal components in an equal-weighted superposition [18–22]. They are crucial elements in quantum metrology [23, 24], quantum optical lithography [25, 26], and quantum information processing [3]. The NOON states have been realized in multiple quantum systems, including polarization states of photons [27], nuclear spin of molecules [28], optical paths of photons [29], ultracold dipolar atoms in an optical superlattice setup [30, 31], and phonons in ion traps [32]. Nevertheless, the multi-step ultra-precise control over the quantum devices, the requirement of the initial states, and the decoherence of quantum systems make it extremely difficult to create and hold entangled states. Fast and convenient protocols for preparing either Bell state or NOON state are still underway.

With unique properties including long coherent time [33–35] and strong and even ultrastrong dipole-dipole coupling [36–40], the circuit-QED system [41, 42] has been used as a promising platform to generate various nonclassical states [5, 43]. Many protocols for generating the entangled states in circuit-QED system have thus been proposed upon the manipulation capability up to the artificial atomic level [36, 37]. It is noted that most of the existing generation protocols [11–14, 44–48] are developed on Rabi oscillations and initialization of the resonator. For example, by tuning the atomic frequency to be resonant with the resonator, the excitation of the artificial atom is transferred to the resonator mode through a half of Rabi oscillation. The NOON state with a significant number N is then generated by a step-by-step processing with resonators prepared as the ground state, that is fragile to both systematic error and environmental noise.

In this work, we propose a two-step protocol for generating the entangled states in a system that two resonators are strongly and dispersively coupled to a superconducting qutrit [36, 37, 41]. The resonators are initially in separable coherent states characterized by complex amplitudes and can be conveniently created by using classical drives [49]. The main ingredient of our protocol relies on the excitation-number-dependent qutrit rotations, allowing for individually manipulating the probability amplitudes of the Fock-state components of coherent states by carefully tailoring the microwave drive signals. The excitation-number-dependent shift in the qutrit transition frequency arises from the dispersive qutrit-resonator interaction [50, 51], which has been applied to realize dressed coherent states [52], entangled states of discrete or discrete-continuous variable systems [53, 54], quantum phase gate [55, 56], and hybrid Fredkin gate [57]. Experimentally it was reported to generate arbitrary Fock states [49] in circuit-QED system.

The rest part of this work is structured as follows. In Sec. II, we introduce our model of two resonators coupled to a Λ-type qutrit and derive the effective Hamiltonian at the dispersive regime. In Sec. III, we provide

* jingjun@zju.edu.cn

a detailed protocol for generating an arbitrary entangled state in Fock space. In Sec. IV A, we analysis the state fidelity of the generation protocol in the presence of un-suppressed state-transitions. The systematic errors from the unstable driving intensity, the decoherence noises for the overall qutrit-resonator system, and the unwanted couplings in the whole system are respectively addressed in Sec. IV B, Sec. IV C, and Sec. IV D. In Sec. V, our generation protocol is extended to adapt to the Ξ-type transmon qutrit. The whole work is summarized in Sec. VI.

II. MODEL AND THE EFFECTIVE HAMILTONIAN

Consider a quantum model that consists of a Λ-type qutrit coupled to two microwave resonators [42] (labeled a and b). The three levels of the qutrit $|g\rangle$, $|e\rangle$, and $|f\rangle$ denote respectively the ground state, the intermediate state, and the highest-level state. The system Hamiltonian ($\hbar = 1$) is given by

$$
\begin{aligned}
H &= H_0 + V, \\
H_0 &= \omega_a a^\dagger a + \omega_b b^\dagger b + \omega_e |e\rangle\langle e| + \omega_f |f\rangle\langle f|, \\
V &= g_a(|f\rangle\langle e| + |e\rangle\langle f|)(a + a^\dagger) \\
&\quad + g_b(|f\rangle\langle g| + |g\rangle\langle f|)(b + b^\dagger),
\end{aligned}
\tag{1}
$$

where ω_a (ω_b) is the transition frequency of the resonator a (b), ω_e (ω_f) represents the free transition frequency of the state $|e\rangle$ ($|f\rangle$), and the ground-state energy is set as zero. The resonator a (b) is coupled to the $|e\rangle \leftrightarrow |f\rangle$ ($|g\rangle \leftrightarrow |f\rangle$) transition in qutrit with the coupling strength g_a (g_b). The two transitions are assumed to be sufficiently detuned or decoupled from each other and then these two couplings can be contributed to independent Rabi transitions.

The interaction Hamiltonian V in Eq. (1) can be considered as a perturbation with respect to the free Hamiltonian H_0, provided that $g_a \ll |\omega_f - \omega_e - \omega_a|$ and $g_b \ll |\omega_f - \omega_b|$. Across the whole Hilbert space, the interaction Hamiltonian would give rise to the energy shift of any eigenstate $|i\rangle$ of the unperturbed Hamiltonian H_0 in Eq. (1). To the second order, the energy shift is effectively given by

$$
\chi = \sum_{j \neq i} \frac{V_{ij} V_{ji}}{\omega_i - \omega_j},
\tag{2}
$$

where $V_{ji} \equiv \langle j|V|i\rangle$ and ω_i is the eigenenergy of $|i\rangle$. For H_0, the eigenstates read $|i\rangle = |gnm\rangle \equiv |g\rangle|n\rangle_a|m\rangle_b$, $|enm\rangle$, and $|fnm\rangle$.

Summarizing the two paths starting from $|gnm\rangle$ and going back to $|gnm\rangle$ through an intermediate state, i.e., $|gnm\rangle \to |fn(m+1)\rangle \to |gnm\rangle$ and $|gnm\rangle \to |fn(m-1)\rangle \to |gnm\rangle$, one can obtain the second-order correction in energy for the state $|gnm\rangle$,

$$
n\omega_a + m\omega_b - m\chi_b - (m+1)\chi_b'
\tag{3}
$$

according to Eq. (2). In the same way, one can obtain the corrected energy for the state $|enm\rangle$

$$
\omega_e + n\omega_a + m\omega_b - n\chi_a - (n+1)\chi_a',
\tag{4}
$$

and the corrected energy for the state $|fnm\rangle$

$$
\omega_f + n\omega_a + m\omega_b + (n+1)\chi_a + n\chi_a' + (m+1)\chi_b + m\chi_b', \tag{5}
$$

where

$$
\begin{aligned}
\chi_a &= \frac{g_a^2}{\omega_f - \omega_e - \omega_a}, \quad \chi_a' = \frac{g_a^2}{\omega_f - \omega_e + \omega_a}, \\
\chi_b &= \frac{g_b^2}{\omega_f - \omega_b}, \quad \chi_b' = \frac{g_b^2}{\omega_f + \omega_b},
\end{aligned}
\tag{6}
$$

are the energy shifts due to the interaction V, describing certain visual two-photon processes in Eq. (2).

It is noted that $|n\rangle$ and $|m\rangle$ are arbitrarily Fock states in the preceding analysis. Thus, in the dispersive regime, i.e., $g_a \ll |\omega_f - \omega_e - \omega_a|$ and $g_b \ll |\omega_f - \omega_b|$, the effective Hamiltonian across the whole Hilbert space can be written as

$$
\begin{aligned}
H_{\text{eff}} &= -\chi_b' |g\rangle\langle g| + (\omega_e - \chi_a') |e\rangle\langle e| \\
&\quad + (\omega_f + \chi_a + \chi_b) |f\rangle\langle f| + \omega_a a^\dagger a + \omega_b b^\dagger b \\
&\quad + (\chi_a + \chi_a') a^\dagger a (|f\rangle\langle f| - |e\rangle\langle e|) \\
&\quad + (\chi_b + \chi_b') b^\dagger b (|f\rangle\langle f| - |g\rangle\langle g|).
\end{aligned}
\tag{7}
$$

The last two lines in the effective Hamiltonian describe the excitation-number-dependent Stark shifts for the atomic levels $|g\rangle$, $|e\rangle$, and $|f\rangle$.

III. TWO-STEP GENERATION PROTOCOL

In this section, we show how to generate an arbitrary entangled state of two resonators in the form of $(|n_1 m_1\rangle + |n_2 m_2\rangle)/\sqrt{2}$, $n_1 \neq n_2$ and $m_1 \neq m_2$, from the coherent states by the effective Hamiltonian in Eq. (7).

Suppose that the qutrit is initially in the superposed state $(|g\rangle + |e\rangle)/\sqrt{2}$ and the two resonators a and b are initially in the coherent state $|\alpha\rangle$ and $|\beta\rangle$, respectively, i.e., the whole system starts from

$$
\begin{aligned}
|\Phi(0)\rangle &= \frac{1}{\sqrt{2}}(|g\rangle + |e\rangle) \otimes |\alpha\rangle \otimes |\beta\rangle, \\
|\alpha\rangle &= e^{-\frac{1}{2}|\alpha|^2} \sum_{n=0}^{\infty} \frac{\alpha^n}{\sqrt{n!}} |n\rangle, \\
|\beta\rangle &= e^{-\frac{1}{2}|\beta|^2} \sum_{m=0}^{\infty} \frac{\beta^m}{\sqrt{m!}} |m\rangle,
\end{aligned}
\tag{8}
$$

where α and β are complex numbers. Alternatively the initial state can be written as

$$
|\Phi(0)\rangle = \mathcal{N} \sum_{n,m}^{\infty} \frac{\alpha^n \beta^m}{\sqrt{n!m!}} (|gnm\rangle + |enm\rangle),
\tag{9}
$$

where $\mathcal{N} = \exp[-(|\alpha|^2 + |\beta|^2)/2]/\sqrt{2}$ is the normalization coefficient. The initial coherent state for the resonator can be achieved by the application of a microwave pulse, that produces a displacement operation $D(\alpha) \equiv \exp(\alpha a^\dagger - \alpha^* a)$ on the vacuum state $|0\rangle$ and $|\alpha\rangle = D(\alpha)|0\rangle$ [49].

Step-1: Applying two $\pi/2$ microwave pulses $\{\Omega, \omega_1\}$ and $\{\Omega, \omega_2\}$ that are nearly resonant with the qutrit transitions $|e\rangle \leftrightarrow |f\rangle$ and $|g\rangle \leftrightarrow |f\rangle$, respectively. Here Ω is the amplitude of the driving pulses satisfying $\Omega T = \pi/2$ with the duration time T and ω_j, $j = 1, 2$, is the driving frequency. The total Hamiltonian including the driving pulses can then be written as

$$\begin{aligned}
H_{\text{tot}} &= H_{\text{eff}} + H_d, \\
H_d &= \Omega\left(|f\rangle\langle e|e^{-i\omega_1 t} + |f\rangle\langle g|e^{-i\omega_2 t} + \text{H.c.}\right).
\end{aligned} \tag{10}$$

In the rotating frame with respect to $U(t) = \exp(iH_{\text{eff}}t)$, the total Hamiltonian turns out to be

$$\begin{aligned}
H'_{\text{tot}} &= U(t)H_{\text{tot}}U^\dagger(t) - iU(t)\dot{U}^\dagger(t) \\
&= \Omega\left(|f\rangle\langle e|e^{i(\omega_{fe} - \omega_1)t} + |f\rangle\langle g|e^{i(\omega_{fg} - \omega_2)t} + \text{H.c.}\right), \\
\omega_{fe} &= \omega_f - \omega_e + (2a^\dagger a + 1)(\chi_a + \chi'_a) \\
&\quad + b^\dagger b(\chi_b + \chi'_b) + \chi_b, \\
\omega_{fg} &= \omega_f + (2b^\dagger b + 1)(\chi_b + \chi'_b) + a^\dagger a(\chi_a + \chi'_a) + \chi_a.
\end{aligned} \tag{11}$$

Consequently, if one chooses

$$\begin{aligned}
\omega_1 &= \omega_f - \omega_e + (2n_1 + 1)(\chi_a + \chi'_a) + m_1(\chi_b + \chi'_b) + \chi_b, \\
\omega_2 &= \omega_f + (2m_2 + 1)(\chi_b + \chi'_b) + n_2(\chi_a + \chi'_a) + \chi_a,
\end{aligned} \tag{12}$$

then in the Fock bases, the total Hamiltonian could be rewritten as

$$\begin{aligned}
H'_{\text{tot}} &= \Omega\left(|fn_1 m_1\rangle\langle en_1 m_1| + |fn_2 m_2\rangle\langle gn_2 m_2|\right) \\
&\quad + \Omega\sum_{n\neq n_1, m\neq m_1}^{\infty} |fnm\rangle\langle enm|e^{i\Delta_{nm}t} \\
&\quad + \Omega\sum_{n\neq n_2, m\neq m_2}^{\infty} |fnm\rangle\langle gnm|e^{i\Delta'_{nm}t} + \text{H.c.},
\end{aligned} \tag{13}$$

where the nonvanishing detunings read

$$\begin{aligned}
\Delta_{nm} &= \omega_f - \omega_e + (2n+1)(\chi_a + \chi'_a) \\
&\quad + m(\chi_b + \chi'_b) + \chi_b - \omega_1, \\
\Delta'_{nm} &= \omega_f + (2m+1)(\chi_b + \chi'_b) + n(\chi_a + \chi'_a) + \chi_a - \omega_2.
\end{aligned} \tag{14}$$

In the ideal weak-driving regime, these detunings Δ_{nm} and Δ'_{nm} are much larger than the Rabi frequency, i.e., $\Delta_{nm}, \Delta'_{nm} \gg \Omega$. In this case, the first driving pulse $\{\Omega, \omega_1\}$ resonantly drives the qutrit transition $|e\rangle \leftrightarrow |f\rangle$ and the resonator modes in the Fock state of $|n_1 m_1\rangle$ and its impact on the other Fock states of resonators could be averaged out in a properly long time-scale. Similarly, the second driving pulse $\{\Omega, \omega_2\}$ resonantly drives the state

transition $|gn_2 m_2\rangle \leftrightarrow |fn_2 m_2\rangle$ and also does not significantly affect the states of resonators other than $|n_2 m_2\rangle$. Using the total Hamiltonian in Eq. (13) under the secular approximation, the initial state of the system $|\Phi(0)\rangle$ thus evolves as

$$\begin{aligned}
|\Phi(t)\rangle &\approx \mathcal{N}\frac{\alpha^{n_1}\beta^{m_1}}{\sqrt{n_1! m_1!}}\left[\cos(\Omega t)|e\rangle - i\sin(\Omega t)|f\rangle\right]|n_1 m_1\rangle \\
&\quad + \mathcal{N}\frac{\alpha^{n_2}\beta^{m_2}}{\sqrt{n_2! m_2!}}\left[\cos(\Omega t)|g\rangle - i\sin(\Omega t)|f\rangle\right]|n_2 m_2\rangle \\
&\quad + \mathcal{N}\sum_{n\neq n_1, m\neq m_1}^{\infty}\frac{\alpha^n\beta^m}{\sqrt{n! m!}}|enm\rangle \\
&\quad + \mathcal{N}\sum_{n\neq n_2, m\neq m_2}^{\infty}\frac{\alpha^n\beta^m}{\sqrt{n! m!}}|gnm\rangle.
\end{aligned} \tag{15}$$

After a period of $\Omega T = \pi/2$, we have

$$\begin{aligned}
|\Phi(T)\rangle &= -i\mathcal{N}\left(\frac{\alpha^{n_1}\beta^{m_1}}{\sqrt{n_1! m_1!}}|fn_1 m_1\rangle + \frac{\alpha^{n_2}\beta^{m_2}}{\sqrt{n_2! m_2!}}|fn_2 m_2\rangle\right) \\
&\quad + \mathcal{N}\sum_{n\neq n_1, m\neq m_1}^{\infty}\frac{\alpha^n\beta^m}{\sqrt{n! m!}}|enm\rangle \\
&\quad + \mathcal{N}\sum_{n\neq n_2, m\neq m_2}^{\infty}\frac{\alpha^n\beta^m}{\sqrt{n! m!}}|gnm\rangle.
\end{aligned} \tag{16}$$

Note it is not necessary to perform the two tailored microwave pulses in the same time. They could be separably applied to the system. We can first drive the transition $|e\rangle \leftrightarrow |f\rangle$ by the microwave pulse $\{\Omega, \omega_1\}$. The total Hamiltonian under the secular approximation is thus described by $\Omega|fn_1 m_1\rangle\langle en_1 m_1| + \text{H.c.}$. Then after a period $\Omega T = \pi/2$, the state $|en_1 m_1\rangle$ evolves into $|fn_1 m_1\rangle$ without involving the other transitions. Next another $\pi/2$ microwave pulse $\{\Omega, \omega_2\}$ is applied to transfer $|gn_2 m_2\rangle$ to $|fn_2 m_2\rangle$. The state in Eq. (16) is eventually achieved.

Step-2: Performing the measurement on the qutrit by the projection operator $M_f = |f\rangle\langle f|$ [58, 59]. Consequently, the reduced density operator of two resonator modes ρ_s becomes

$$\rho_s(T) = \text{Tr}_q\left[\frac{M_f|\Phi(T)\rangle\langle\Phi(T)|M_f}{\text{Tr}[M_f|\Phi(T)\rangle\langle\Phi(T)|M_f]}\right] = |\phi\rangle\langle\phi|, \tag{17}$$

where the denominator $P = \text{Tr}[M_f|\Phi(T)\rangle\langle\Phi(T)|M_f]$ is the success probability [60, 61] and Tr_q means partial trace over the qutrit. Up to a dynamical phase accumulated in the evolution, $|\phi\rangle$ is a desired entangled state fully determined by $n_{1,2}$ and $m_{1,2}$ selected in Eq. (12),

$$|\phi\rangle = \cos\varphi|n_1 m_1\rangle + \sin\varphi|n_2 m_2\rangle, \tag{18}$$

where

$$\tan\varphi = \frac{\alpha^{n_2}\beta^{m_2}\sqrt{n_1! m_1!}}{\alpha^{n_1}\beta^{m_1}\sqrt{n_2! m_2!}}. \tag{19}$$

A balanced superposition requires that $\tan\varphi = 1$. Note hereafter both α and β are supposed to be positive numbers for simplicity. On this stage, we have generated an arbitrary entangled state of two continuous-variable modes with a success probability

$$P = \mathcal{N}^2 \left(\frac{\alpha^{2n_1}\beta^{2m_1}}{n_1! m_1!} + \frac{\alpha^{2n_2}\beta^{2m_2}}{n_2! m_2!} \right) \quad (20)$$

according to Eqs. (16) and (17).

Here are two distinguishing instances. With $n_1 = m_1 = 0$ and $n_2 = m_2 = 1$, one can obtain the double-excitation Bell state

$$|\phi\rangle = \frac{1}{\sqrt{2}}(|00\rangle + |11\rangle) \quad (21)$$

by setting the coherent-state parameters as $\alpha = \beta = 1$. With $n_1 = m_2 = 0$, $m_1 = n_2 = N$, and $\alpha = \beta$, the entangled state in Eq. (18) turns out to be a NOON state

$$|\phi\rangle = \frac{1}{\sqrt{2}}(|0N\rangle + |N0\rangle). \quad (22)$$

The efficiency of our protocol for generating $|\phi\rangle$ can be qualified by the state fidelity

$$F = \frac{\langle\phi|\langle f|\rho(T)|f\rangle|\phi\rangle}{\mathrm{Tr}[M_f\rho(T)M_f]}. \quad (23)$$

where $\rho(T)$ is the density matrix directly obtained by Eq. (13) without the secular approximation. We also ignore the dynamical phase of the time-evolved state in practical numerical simulation.

IV. FIDELITY ANALYSIS

A. Undesired transition in the presence of driving

The state evolution under the secular approximation in Step-1 of Sec. III reflects the ideal assumption that the microwave driving pulses can only affect the desired pairs of states $\{n_1, m_1\}$ and $\{n_2, m_2\}$ filtered out by choosing the driving frequency in Eq. (12). However, the two driving pulses might inevitably induce the other state transitions that might invalidate the secular-approximation condition $\Delta_{nm}, \Delta'_{nm} \gg \Omega$. In the following we calculate the state fidelity (23) by considering the impact from the unwanted evolution induced by vanishing Δ_{nm} and Δ'_{nm}.

The total Hamiltonian in Eq. (13) is block-diagonal in terms of the subspaces spanned by $\{|fnm\rangle, |enm\rangle\}$ and $\{|fnm\rangle, |gnm\rangle\}$ with arbitrary pairs of Fock state $|nm\rangle$. Then in any subspace of $\{|fnm\rangle, |enm\rangle\}$, the total Hamiltonian can be effectively described (through rotating to a frame with time-independent coefficients) as

$$H = \begin{bmatrix} \Delta_{nm} & \Omega \\ \Omega & 0 \end{bmatrix} = \frac{\Delta_{nm}}{2}\hat{I} + \begin{bmatrix} \frac{\Delta_{nm}}{2} & \Omega \\ \Omega & -\frac{\Delta_{nm}}{2} \end{bmatrix}, \quad (24)$$

where $\hat{I}$ is a two-dimensional identity operator and Δ_{nm} is already given by Eq. (14). The local time evolution operator reads,

$$U = \cos(E_{nm}t)\hat{I} - i\sin(E_{nm}t)\begin{bmatrix} \cos(2\theta_{nm}) & \sin(2\theta_{nm}) \\ \sin(2\theta_{nm}) & -\cos(2\theta_{nm}) \end{bmatrix},$$
$$E_{nm} = \sqrt{\Omega^2 + (\Delta_{nm}/2)^2},$$
$$\tan(2\theta_{nm}) = 2\Omega/\Delta_{nm}. \quad (25)$$

Then for the initial state $|\psi(0)\rangle = |enm\rangle$, we have

$$|\psi(t)\rangle = -i\sin(E_{nm}t)\sin(2\theta_{nm})|fnm\rangle \\ + [\cos(E_{nm}t) + i\sin(E_{nm}t)\cos(2\theta_{nm})]|enm\rangle. \quad (26)$$

At the measurement time satisfying $\Omega T = \pi/2$ in Step-2 of Sec. III, the population on the state $|nm\rangle$ of the resonators is found to be $P_{nm} = \sin^2(E_{nm}T)\sin^2(2\theta_{nm})$. The time evolution in the subspace $\{|fnm\rangle, |gnm\rangle\}$ can be calculated in a similar way. Then the population on the state $|nm\rangle$ at the time $t = T = \pi/(2\Omega)$ is $P'_{nm} = \sin^2(E'_{nm}T)\sin^2(2\theta'_{nm})$, where E'_{nm} and $\tan(2\theta'_{nm})$ are obtained through Eq. (25) by replacing Δ_{nm} with Δ'_{nm}.

Across all these separable subspaces, the fidelity of the desired entangled-state indicated by $\{n_1, m_1\}$ and $\{n_2, m_2\}$ given the initial state $|\Phi(0)\rangle$ in Eq. (9) is found to be

$$F = \frac{\frac{\alpha^{2n_1}\beta^{2m_1}}{\sqrt{n_1! m_1!}} + \frac{\alpha^{2n_2}\beta^{2m_2}}{\sqrt{n_2! m_2!}}}{\sum_{n,m} \frac{\alpha^{2n}\beta^{2m}}{\sqrt{n! m!}}(P_{nm} + P'_{nm})} \quad (27)$$

according to Eq. (23). Note $P_{n_1 m_1} = P'_{n_2 m_2} = 1$.

This result is consistent with the condition that both $\Delta_{n\neq n_1, m\neq m_1}$ and $\Delta'_{n\neq n_2, m\neq m_2}$ should be sufficiently larger than Ω, on which an ignorable weight of the unwanted evolutions yields an desired entangled state with a high fidelity. However, this condition cannot be always satisfied for arbitrary $|nm\rangle$. Due to Eqs. (12) and (14), certain detunings $\Delta_{n'_1 m'_1}$ and $\Delta'_{n'_2 m'_2}$ will approach vanishing when the Fock states indicated by $\{n'_1, m'_1\}$ and $\{n'_2, m'_2\}$ satisfy

$$\omega_1 \approx \omega_f - \omega_e + (2n'_1 + 1)(\chi_a + \chi'_a) \\ + m'_1(\chi_b + \chi'_b) + \chi_b, \\ \omega_2 \approx \omega_f + (2m'_2 + 1)(\chi_b + \chi'_b) + n'_2(\chi_a + \chi'_a) + \chi_a, \quad (28)$$

the same as the desired pairs of $\{n_1, m_1\}$ and $\{n_2, m_2\}$.

If the coupling strength between qutrit and resonators is sufficiently weak, e.g., $g_{a,b} \sim 0.01\omega_{a,b}$, then the energy shifts $\chi'_{a,b}$ induced by the counterrotating interactions $|f\rangle\langle e|a^\dagger + \mathrm{H.c.}$ and $|f\rangle\langle g|b^\dagger + \mathrm{H.c.}$ would be much less than the energy shifts $\chi_{a,b}$ induced by the rotating-wave interactions $|e\rangle\langle f|a^\dagger + \mathrm{H.c.}$ and $|g\rangle\langle f|b^\dagger + \mathrm{H.c.}$ as implied by Eq. (6). It is then straightforward to find that Eq. (28) can be met under the conditions

$$n'_1 = n_1 + n_k, \quad n'_2 = n_2 + n'_k, \\ m'_1 = m_1 - m_k, \quad m'_2 = m_2 - m'_k, \\ \frac{m_k}{2n_k} \approx \frac{\chi_a}{\chi_b}, \quad \frac{n'_k}{2m'_k} \approx \frac{\chi_b}{\chi_a}, \quad (29)$$

where n_k, m_k, n'_k, and m'_k are nonnegative integers representing the shifts from the desired Fock state implied by $\{n_1, m_1\}$ and $\{n_2, m_2\}$. In other words, the states $|en'_1 m'_1\rangle$ ($|gn'_2 m'_2\rangle$) would evolve to $|fn'_1 m'_1\rangle$ ($|fn'_2 m'_2\rangle$) in parallel to the wanted transition $|en_1 m_1\rangle \rightarrow |fn_1 m_1\rangle$ ($|gn_2 m_2\rangle \rightarrow |fn_2 m_2\rangle$) with a nonnegligible probability under the same driving H_d in Eq. (10).

To reduce the probability of the unwanted state transitions, one can properly choose χ_a and χ_b so that the populations on the states $|n'_1 m'_1\rangle$ and $|n'_2 m'_2\rangle$ are significantly smaller than those of $|n_1 m_1\rangle$ and $|n_2 m_2\rangle$. Apparently, this requirement can be satisfied when the shift ratios m_k/n_k and m'_k/n'_k are irreducible ratios of large integers that are much larger than the average number of excitations for the fixed initial coherent states, i.e., $|\alpha|^2$ or $|\beta|^2$. According to the results in Eq. (6), the ratio of energy shifts χ_a/χ_b are determined by the transition frequencies of the qutrit and two resonators as

$$\frac{\chi_a}{\chi_b} = \frac{\omega_f - \omega_b}{\omega_f - \omega_e - \omega_a}, \tag{30}$$

under the condition that the coupling strengths are isotropic $g_a = g_b = g$. The ratio is thus an important element to the state fidelity, which can be properly adjusted by the frequencies of the system components. Its value should not be in the proximity of an irreducible ratio of small integers.
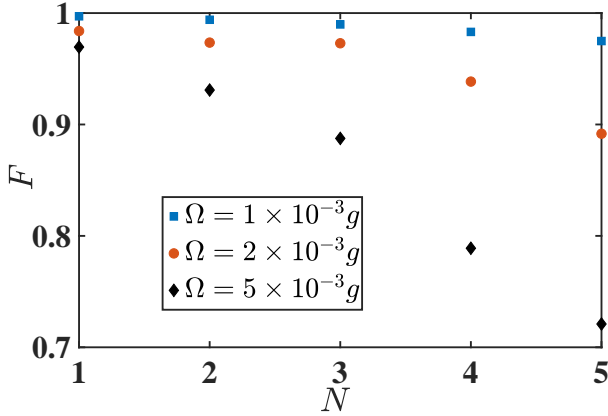

FIG. 1. Fidelity of the NOON state $(|0N\rangle + |N0\rangle)/\sqrt{2}$ as a function of N under various Rabi frequencies Ω. The parameters are set as $\alpha = \beta = 1$, $g_a = g_b = g$, $\omega_e = 20g$, $\omega_f = 100g$, $\omega_a = 70g$ and $\omega_b = 89g$.

Figure 1 confirms our two-step protocol in generating the NOON state from coherent states with $\alpha = \beta = 1$. We plot the state fidelity obtained by Eq. (23) or Eq. (27) under various Rabi frequencies Ω of the driving pulses in the total Hamiltonian (13). As the preceding analyse, the fidelities decline with increasing Ω for arbitrary N. For example, the fidelity for the NOON state of $N = 2$ is 0.994 when $\Omega = 1 \times 10^{-3}g$ and it declines to 0.938 when the Rabi frequency is enhanced to $\Omega = 5 \times 10^{-3}g$. In addition, one can find a larger N gives rise to a smaller fidelity and the decline magnitude increases under larger

Ω. In comparison to the state of $N = 2$, the fidelity of the state of $N = 5$ declines from 0.970 ($\Omega = 1 \times 10^{-3}g$) to 0.721 ($\Omega = 5 \times 10^{-3}g$).
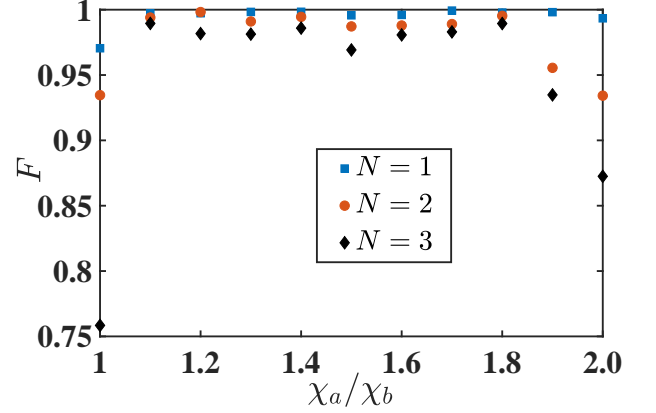

FIG. 2. Fidelity of the NOON state $(|0N\rangle + |N0\rangle)/\sqrt{2}$ as a function of the ratio of energy shifts χ_a/χ_b under various N. The transition frequency ω_e is changed to manipulate χ_a/χ_b. The other parameters are the same as Fig. 1.

To avoid the participation of the unwanted state transition involving $|n'_1 m'_1\rangle$ and $|n'_2 m'_2\rangle$, the ratio of χ_a/χ_b in Fig. 1 is set to be $11/10$. Both numerator and denominator are faraway from either $|\alpha|^2$ or $|\beta|^2$. In Fig. 2, we plot the NOON state fidelity as a function of χ_a/χ_b in the range of $[1, 2]$. As expected, the fidelity declines as the increasing of the Fock number N. More importantly, one can observe that the fidelity declines significantly at certain values that could be expressed by irreducible ratio of small integers, e.g., $\chi_a/\chi_b = 1$, $\chi_a/\chi_b = 1.5$, and $\chi_a/\chi_b = 2$. It can be theoretically explained by Eq. (29). For example, $\chi_a/\chi_b = 1$ gives rise to $m_k/n_k = 2$. Under this condition, in parallel to the desired state transition $|e10\rangle \rightarrow |f10\rangle$, we have an unwanted evolution described by $|e02\rangle \rightarrow |f02\rangle$ under the total Hamiltonian (13). Similarly, the populations on the states $|e12\rangle$ and $|e04\rangle$ cannot be ignored if the target transition is $|e20\rangle \rightarrow |f20\rangle$. In contrast, the fidelities are nearly unit at the other points, e.g., $\chi_a/\chi_b = 1.1$ and $\chi_a/\chi_b = 1.7$. In these cases, the populations of unwanted states $|en'_1 m'_1\rangle$ satisfying the condition presented in Eq. (29) are significant smaller than the population of the target-state $|en_1 m_1\rangle$, regarding $|\alpha = 1\rangle$. Thus, a high-fidelity entangled state can be achieved by properly choosing the initial coherent states of the resonator and the frequencies of ancillary qutrit.

B. Systematic errors on driving intensity

From Eqs. (15) and (16), it is important for our protocol to perform the measurement at the keypoint $\Omega t = \pi/2$. Then it seems that the driving intensities Ω for both $|f\rangle\langle e|$ and $|f\rangle\langle g|$ have to take the same magnitude. The ideal control parameters might not be exactly implemented because of the technical imperfections and

constrains. In this subsection, we consider the systematic errors raised by the unequal driving amplitudes. In particular, they are assumed to be departed from each other by a relative magnitude ϵ.

In particular, the driving Hamiltonian in Eq. (10) is rewritten as

$$H_d = \Omega \left[(1 - \epsilon)|f\rangle\langle e|e^{-i\omega_1 t} + (1 + \epsilon)|f\rangle\langle g|e^{-i\omega_2 t} + \text{H.c.} \right].$$
(31)

and consequently the total Hamiltonian (13) in rotating frame becomes

$$\begin{aligned}
H_{\text{err}} &= \Omega(1 - \epsilon)|fn_1m_1\rangle\langle en_1m_1| \\
&+ \Omega(1 + \epsilon)|fn_2m_2\rangle\langle gn_2m_2| \\
&+ \Omega(1 - \epsilon) \sum_{n\neq n_1, m\neq m_1}^{\infty} |fnm\rangle\langle enm|e^{i\Delta_{nm}t} \\
&+ \Omega(1 + \epsilon) \sum_{n\neq n_2, m\neq m_2}^{\infty} |fnm\rangle\langle gnm|e^{i\Delta'_{nm}t} + \text{H.c.}.
\end{aligned}$$
(32)

With the Hamiltonian in Eq. (32), the initial state $|\Phi(0)\rangle$ in Eq. (9) evolves to

$$\begin{aligned}
&|\Phi(T)\rangle \\
&\approx \mathcal{N}\frac{\alpha^{n_1}\beta^{m_1}}{\sqrt{n_1!m_1!}} \left[\sin\left(\frac{\pi\epsilon}{2}\right)|e\rangle - i\cos\left(\frac{\pi\epsilon}{2}\right)|f\rangle \right]|n_1m_1\rangle \\
&- \mathcal{N}\frac{\alpha^{n_2}\beta^{m_2}}{\sqrt{n_2!m_2!}} \left[\sin\left(\frac{\pi\epsilon}{2}\right)|g\rangle + i\cos\left(\frac{\pi\epsilon}{2}\right)|f\rangle \right]|n_2m_2\rangle \\
&+ \mathcal{N} \sum_{n\neq n_1, m\neq m_1}^{\infty} \frac{\alpha^n\beta^m}{\sqrt{n!m!}}|enm\rangle \\
&+ \mathcal{N} \sum_{n\neq n_2, m\neq m_2}^{\infty} \frac{\alpha^n\beta^m}{\sqrt{n!m!}}|gnm\rangle,
\end{aligned}$$
(33)

at the desired moment $\Omega T = \pi/2$. Then we measure the qutrit with the projection operator M_f, one can still obtain the (unnormalized) target state

$$|\phi\rangle = \cos\left(\frac{\pi\epsilon}{2}\right) [\cos\varphi|n_1m_1\rangle + \sin\varphi|n_2m_2\rangle].$$
(34)

Since $\cos(\pi\epsilon/2)$ is a common factor, the error ϵ on driving intensity can therefore be ignored in the ideal situation that the microwave pulses only drive the desired states. Its effect, however, will emerge when considering the unwanted evolution induced by vanishing Δ_{nm} and Δ'_{nm} as discussed in Sec. IV A.

Under the Hamiltonian (32) with the systematic error ϵ, the fidelities of the double-excitation Bell state $(|00\rangle + |11\rangle)/\sqrt{2}$ and the NOON state $(|0N\rangle + |N0\rangle)/\sqrt{2}$ are presented in Fig. 3 and Fig. 4, respectively, as a function of ϵ. The fidelities are evaluated at the desired moment $\Omega T = \pi/2$ as requested by Step-2 of our protocol.

It is found in Fig. 3, that the fidelity sensitivity to the driving error ϵ is increased with increasing Rabi frequency Ω. In particular, for $\Omega = 1 \times 10^{-3}g$, the fidelities are roughly invariant in the presence of ϵ, even when it is
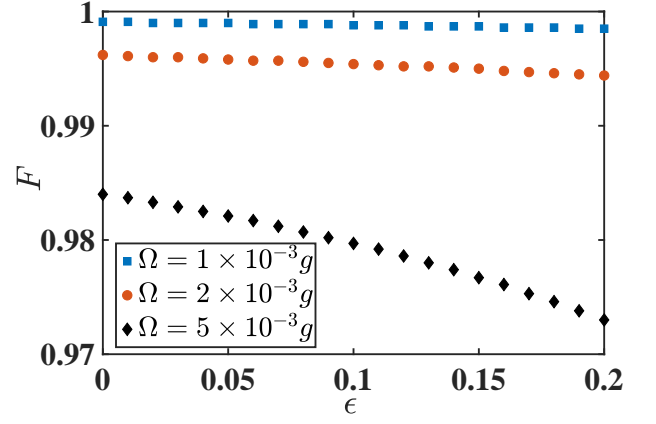

FIG. 3. Fidelity of the double-excitation Bell state $(|00\rangle + |11\rangle)/\sqrt{2}$ as a function of the systematic error ϵ. The parameters are the same as Fig. 1.
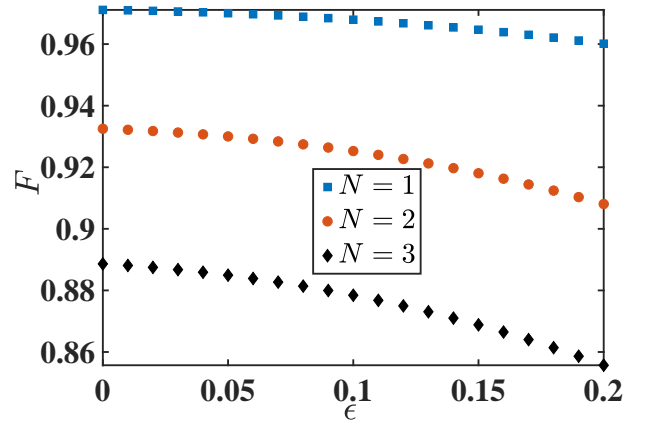

FIG. 4. Fidelity of the NOON state $(|0N\rangle + |N0\rangle)/\sqrt{2}$ as a function of the systematic error ϵ under various N. $\Omega = 5 \times 10^{-3}g$ and the other parameters are the same as Fig. 1.

about 20%. And for $\Omega = 5 \times 10^{-3}g$, it is slightly declined when ϵ increases from 0 to 20%. This result could be understood since the condition $\Omega(1 + \epsilon) \ll \chi_a, \chi_b$ becomes less robust for larger Ω. In Fig. 4, the results for various N are obtained under $\Omega = 5 \times 10^{-3}g$. Although larger N gives rise to larger decreasing amplitude, the fidelities can still be maintained over 0.86 with about 20% errors in the driving intensity. Thus, one can conclude that our entangled-state generation protocol is robust against the fluctuations on the Rabi frequencies. We can have a high fidelity as long as the measurement moment is determined by the average value of these Rabi frequencies.

C. External decoherence

In state generation process, the composite system we considered cannot be completely isolated from the surrounding environment. The target entangled state will be damaged by the influence from both resonator damp-

ing and qutrit decoherence. Taking the local decoherence channels into consideration, we can study the entangled state generation fidelity in a standard open-quantum-system framework. Under the Markovian approximation and tracing out the degrees of freedom of the external environments (assumed to be at the vacuum states), we arrive at the master equation for the density operator $\rho(t)$ of the full system consisting of qutrit and resonators

$$\dot{\rho}(t) = -i\left[H'_{\text{tot}}, \rho(t)\right] + \kappa_a \mathcal{L}[a] + \kappa_b \mathcal{L}[b] + \gamma_{fe} \mathcal{L}[|e\rangle\langle f|] + \gamma_{fg} \mathcal{L}[|g\rangle\langle f|].$$
(35)

Here H'_{tot} is the total Hamiltonian in Eq. (13). κ_a (κ_b) is the decay constant of the resonator mode a (b). γ_{fe} and γ_{fg} are the energy relaxation constants associated with the transitions $|f\rangle \rightarrow |e\rangle$ and $|f\rangle \rightarrow |g\rangle$, respectively. For simplicity, these decay rates are assumed to take the same value γ. The Lindblad superoperator $\mathcal{L}$ is defined as

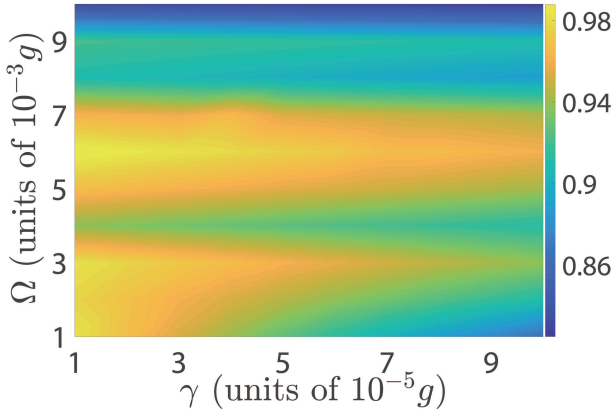$$\mathcal{L}[o] \equiv o\rho o^\dagger - \frac{1}{2}o^\dagger o\rho - \frac{1}{2}\rho o^\dagger o.$$
(36)

FIG. 5. Fidelity of the Bell state $(|01\rangle + |10\rangle)/\sqrt{2}$ in the parametric space of Rabi frequencies Ω and decoherence rates γ. The other parameters are the same as Fig. 1.

The fidelities of the target state $(|01\rangle + |10\rangle)/\sqrt{2}$ under various Rabi frequencies Ω and decoherence rates γ are shown in Fig. 5. In the presence of a larger decoherence rate γ, one can observe that a smaller Rabi frequency Ω does not always yields a higher fidelity as in Figs. (1) and (3). We have to make a compromise of Ω to optimize the fidelity due to the fact that the desired period T of the state generation is inversely proportional to the Ω and the dissipation becomes more severe under a longer evolution time. It is found that the fidelity in two optimized regimes is maintained above 0.95. One is around $5 \times 10^{-3}g < \Omega < 7 \times 10^{-3}g$ even when γ is nearly $10^{-4}g$; another one is around $1 \times 10^{-3}g < \Omega < 3 \times 10^{-3}g$ when $\gamma < 3 \times 10^{-5}g$.

In Fig. 6, we present the impact of decoherence on the NOON state fidelity under $\Omega = 1 \times 10^{-3}g$. As expected,
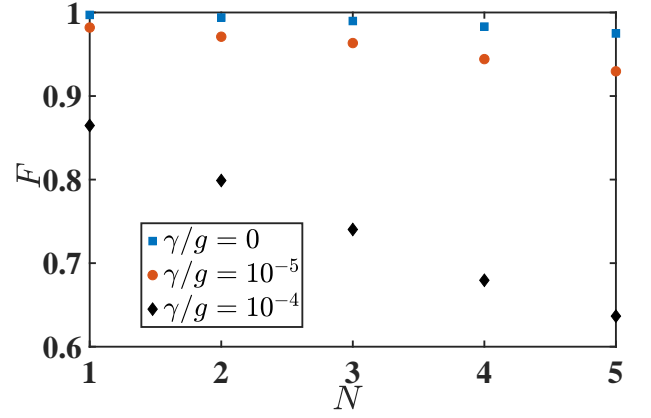

FIG. 6. Fidelity of the NOON state $(|0N\rangle + |N0\rangle)/\sqrt{2}$ as a function of N under various decoherence rates. $\Omega = 1 \times 10^{-3}g$ and the other parameters are the same as Fig. 1.

one can observe that the fidelity declines with the increasing Fock number N. With a moderate decoherence rate $\gamma/g = 10^{-5}$, the fidelities are 0.982, 0.971, 0.963, 0.944, and 0.93 for $N = 1, 2, 3, 4, 5$, respectively. And under a stronger decoherence rate $\gamma/g = 10^{-4}$, the NOON state fidelity declines to 0.637 for $N = 5$.

In a typical system that consisting of a flux qutrit and two resonators [33, 35, 36, 41], the transition frequencies among the lowest three levels of the qutrit can be manipulated within the range of $[1, 20]$ GHz, and the frequencies of the resonators are in the order of ~ 10 GHz. The coupling between the qutrit and resonators has entered the strong and even ultrastrong coupling regimes [36, 37], i.e., $g/\omega \sim 0.01 - 0.1$. The coherence timescale of the qutrit is about $\gamma^{-1} \sim 10\mu s$ and the quality factor of the resonators is about $Q \sim 10^6 - 10^7$ [42]. The decay rate is then about $\gamma/g \sim 10^{-5}-10^{-4}$ as we used in the preceding numerical calculations.

D. Unwanted couplings

In addition to the external noises, the whole system could be also subject to the influence from unwanted couplings inside the system. In a superconducting circuit platform, the lowest three levels actually constitute a Δ-type qutrit [41, 42] for $\Phi/\Phi_0 \neq 1/2$, where Φ is the static magnetic flux applied to the loop and Φ_0 is the magnetic-flux quantum. With suitable parameters in junction, the dipole-dipole transition rates in the flux qutrit satisfy $\gamma_{fg}, \gamma_{fe} \gg \gamma_{eg}$ [41]. Then the elements in the transition matrix describing $|f\rangle \leftrightarrow |e\rangle$ and $|f\rangle \leftrightarrow |g\rangle$ are dominant over that for $|e\rangle \leftrightarrow |g\rangle$ in amplitude. The Δ-type could thus be approximated as the Λ-type. However, the transition between levels $|e\rangle \leftrightarrow |g\rangle$ is unavoidable. Its effect thus should be considered in practice.

With a Δ-type qutrit in our model, the interaction Hamiltonian V in the initial Hamiltonian (1) should be

replaced by

$$\tilde{V} = [g_a(a^\dagger + a) + g_b(b + b^\dagger)] \times$$
$$(|e\rangle\langle g| + |g\rangle\langle e| + |f\rangle\langle e| + |e\rangle\langle f| + |f\rangle\langle g| + |g\rangle\langle f|), \tag{37}$$

where the coupling strengths between any transitions and resonators are supposed to be the same to simplify the discussion but with no loss of generality. With the second-perturbation method presented in Eq. (2), the effective Hamiltonian in Eq. (7) for the whole system is modified to

$$\tilde{H}_{\text{eff}} = \sum_{k,j\in g,e,f,l\in a,b} \left[\omega_k + \Theta(kj)\chi_{kj}^l \right] |k\rangle\langle k|$$
$$+ \sum_{k,j\in g,e,f,l\in a,b} \chi_{kj}^l l^\dagger l \Theta(kj) \left(|k\rangle\langle k| - |j\rangle\langle j| \right), \tag{38}$$

where the energy shifts read

$$\chi_{kj}^l = \frac{g_l^2}{\Theta(kj)(\omega_k - \omega_j - \omega_l)}. \tag{39}$$

We here employ the step function $\Theta(kj)$, i.e., $\Theta(kj) = -1$ when $\omega_k < \omega_j$ and $\Theta(kj) = 1$ when $\omega_k > \omega_j$.

The driving Hamiltonian H_d in Eq. (10) is still applicable to filter out the desired state transitions indicated by $|en_1m_1\rangle \to |fn_1m_1\rangle$ and $|gn_2m_2\rangle \to |fn_2m_2\rangle$. Under the modified effective Hamiltonian in Eq. (38), it is found that the two frequencies of microwave pulses are modified to

$$\tilde{\omega}_1 = \omega_f - \omega_e + (2n_1+1)(\chi_{ef}^a + \chi_{fe}^a) + n_1(\chi_{gf}^a - \chi_{ge}^a)$$
$$+ (n_1+1)(\chi_{fg}^a - \chi_{eg}^a) + (2m_1+1)(\chi_{ef}^b + \chi_{fe}^b)$$
$$+ m_1(\chi_{gf}^b - \chi_{ge}^b) + (m_1+1)(\chi_{fg}^b - \chi_{eg}^b),$$
$$\tilde{\omega}_2 = \omega_f + (2n_2+1)(\chi_{gf}^a + \chi_{fg}^a) + n_2(\chi_{ef}^a + \chi_{eg}^a)$$
$$+ (n_2+1)(\chi_{fe}^a + \chi_{ge}^a) + (2m_2+1)(\chi_{gf}^b + \chi_{fg}^b)$$
$$+ m_2(\chi_{ef}^b + \chi_{eg}^b) + (m_2+1)(\chi_{fe}^b + \chi_{ge}^b). \tag{40}$$

The total Hamiltonian in analog to Eq. (10) is then written as

$$\tilde{H}_{\text{tot}} = \tilde{H}_{\text{eff}} + H_d. \tag{41}$$

Next one can carry out a similar rotation as in Step-1 in our protocol to obtain the desired time-independent Hamiltonian Eq. (13). Under the secular approximation, it is used to push the system into the required state in Eq. (16) for Step-2.

It is straightforward to check that the transition frequencies ω_1 and ω_2 in Eq. (12) could be respectively recovered by $\tilde{\omega}_1$ and $\tilde{\omega}_2$ when the energy shifts $\chi_{fe}^a \gg \chi_{eg}^a, \chi_{fg}^a$ and $\chi_{fg}^b \gg \chi_{eg}^b, \chi_{fe}^b$. Consequently, the Δ-type qutrit is approximated by the Λ-type qutrit discussed in Sec. II. In this case, $\chi_{fe}^a = \chi_a$, $\chi_{ef}^a = \chi_a'$, $\chi_{fg}^a = \chi_b$, and $\chi_{gf}^b = \chi_b'$, where χ_a, χ_a', χ_b, and χ_b' have been given in Eq. (6).
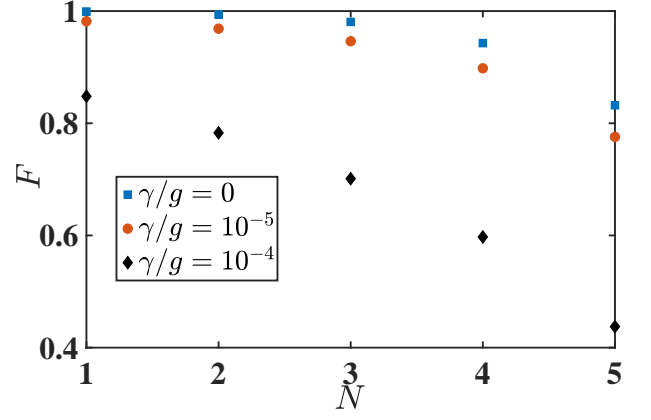

FIG. 7. Fidelity of the NOON state $(|0N\rangle + |N0\rangle)/\sqrt{2}$ as a function of N under the Hamiltonian $\tilde{H}_{\text{tot}}$ for the Δ-type qutrit. The parameters are the same as Fig. 6.

In Fig. 7, we present the NOON state fidelity by using the Lindblad master equation (35) with the modified total Hamiltonian $\tilde{H}_{\text{tot}}$. Also the extra decoherence channel described by $\mathcal{L}[|g\rangle\langle e|]$ is added into Eq. (35) with the same dissipation rate γ. In contrast to Fig. 5, one can observe that all of the fidelities for the Δ-type qutrit are smaller than their relevant results for the Λ-type one. In particular, the fidelities are 0.982, 0.969, 0.946, 0.898, and 0.778 for $N = 1,2,3,4,5$, respectively, under $\gamma/g = 10^{-5}$. And under a stronger decoherence for $\gamma/g = 10^{-4}$, they decline to 0.848, 0.783, 0.701, 0.597, and 0.438, respectively. The unwanted coupling in real experiments is thus harmful to our entangled-state generating protocol.
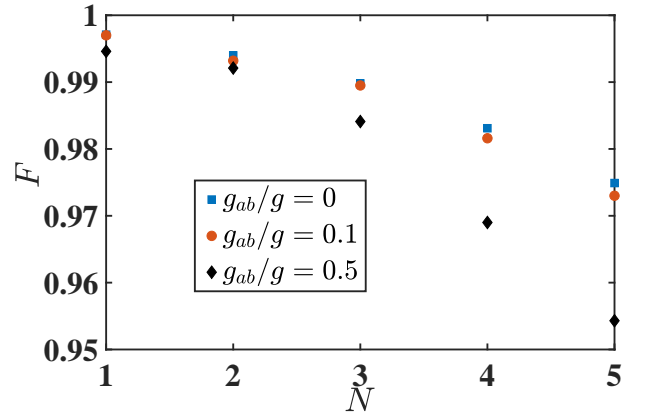

FIG. 8. Fidelity of the NOON state $(|0N\rangle + |N0\rangle)/\sqrt{2}$ as a function of N under various strength of crosstalk g_{ab} between two resonators. $\Omega = 1 \times 10^{-3}g$ and the other parameters are the same as Fig. 1.

Another unwanted coupling arises from the crosstalk between the two resonators a and b. In this situation, the interaction Hamiltonian V in Eq. (1) becomes

$$\tilde{V} = V + g_{ab}(a + a^\dagger)(b + b^\dagger), \tag{42}$$

where g_{ab} is the inter-resonator coupling strength. Accordingly, the total Hamiltonian in Eq. (13) turns out to be

$$\tilde{H}_{\text{tot}} = H'_{\text{tot}} + g_{ab}(a + a^\dagger)(b + b^\dagger). \tag{43}$$

In Fig. 8, the NOON state fidelities under various crosstalk coupling strength g_{ab} are calculated in the absence of decoherence. The crosstalk is also found to be a harmful ingredient to the fidelity of the generated state for any N. Yet its effect is not significant. For $N = 5$, comparing to $F = 0.975$ when $g_{ab} = 0$, the fidelity can be maintained as $F = 0.954$ even when $g_{ab} = 0.5g$.

V. DISCUSSION

In addition to the Δ-type qutrit for $\Phi/\Phi_0 \neq 1/2$ as discussed in Sec IV D, our protocol can be implemented by a Ξ-type transmon qutrit at the specific ratio $\Phi/\Phi_0 = 1/2$. In this case, the full Hamiltonian in Eq. (1) could be rewritten as

$$\begin{aligned}
H &= H_0 + V, \\
H_0 &= \omega_a a^\dagger a + \omega_b b^\dagger b + \omega_e |e\rangle\langle e| + \omega_f |f\rangle\langle f|, \\
V &= g_a(|e\rangle\langle g| + |g\rangle\langle e|)(a + a^\dagger) \\
&\quad + g_b(|f\rangle\langle e| + |e\rangle\langle f|)(b + b^\dagger).
\end{aligned} \tag{44}$$

In the absence of unwanted inner transition between $|g\rangle$ and $|f\rangle$ and the crosstalk between the two resonators, the effective Hamiltonian in the dispersive regime (7) under the second-order perturbation (2) becomes,

$$\begin{aligned}
H_{\text{eff}} &= -\chi'_a|g\rangle\langle g| + (\omega_e + \chi_a - \chi'_b)|e\rangle\langle e| \\
&\quad + (\omega_f + \chi_b)|f\rangle\langle f| + \omega_a a^\dagger a + \omega_b b^\dagger b \\
&\quad + (\chi_a + \chi'_a)a^\dagger a(|e\rangle\langle e| - |g\rangle\langle g|) \\
&\quad + (\chi_b + \chi'_b)b^\dagger b(|f\rangle\langle f| - |e\rangle\langle e|).
\end{aligned} \tag{45}$$

where

$$\begin{aligned}
\chi_a &= \frac{g_a^2}{\omega_e - \omega_a}, \quad \chi'_a = \frac{g_a^2}{\omega_e + \omega_a}, \\
\chi_b &= \frac{g_b^2}{\omega_f - \omega_e - \omega_b}, \quad \chi'_b = \frac{g_b^2}{\omega_f - \omega_e + \omega_b}.
\end{aligned} \tag{46}$$

The effective Hamiltonian describes also the photon-number-dependent Stark shifts for each energy levels

of qutrit. Following the same procedure illustrated in Sec. III, we can convert the initial state $(|g\rangle + |f\rangle)/\sqrt{2} \otimes |\alpha\rangle|\beta\rangle$ into a desired entangled state, by using two tailored microwave pulses transferring the states $|gn_1m_1\rangle \rightarrow |en_1m_1\rangle$ and $|fn_2m_2\rangle \rightarrow |en_2m_2\rangle$ and then measuring the qutrit with the projection operator $M_e = |e\rangle\langle e|$.

VI. CONCLUSION

In summary, we have presented a concise two-step protocol for creating arbitrary entangled states in a setup consisting of two microwave resonators strongly coupled to a Λ-type qutrit. No extra steps have to be taken to shape the initial coherent states of the resonator. With a second-order perturbation method, the system could be described by an effective Hamiltonian at the dispersive regime. We take advantage over the fact that the shifts of the qutrit transition frequencies are excitation-number-dependent. It allows to apply tailored microwave drive signals to individually control the qutrit transition amplitudes associated with the desired Fock states. Then the entangled states of the two resonators could be generated by a typical evolution-and-measurement procedure, merely using their initial coherent states. In the presence of strong driving, we presented the generating fidelity and found that the undesired state transitions can be suppressed by properly choosing the transition frequencies of system components. Moreover, our protocol is found to be robust against the systematic errors arising from the microwave driving intensity, the quantum decoherence of all components, and the crosstalk of two resonators. Our protocol can be extended to the three-level qutrits in both Δ and Ξ configurations. Hence, our study is of interest in the pursuit of the entangled state of continuous-variable systems with the dispersive interaction and finds important applications in the state manipulation of the circuit-QED system with less steps.

[1] R. Horodecki, P. Horodecki, M. Horodecki, and K. Horodecki, *Quantum Entanglement,* Rev. Mod. Phys. **81**, 865 (2009).

[2] N. Gisin and R. Thew, *Quantum Communication,* Nat. Photon. **1**, 165 (2007).

[3] C. H. Bennett and B. D. DiVincenzo, *Quantum Information and Computation,* Natrue **404**, 247 (2000).

[4] K. Mølmer and A. Sørensen, *Multiparticle entanglement of hot trapped ions,* Phys. Rev. Lett. **82**, 1835 (1999).

[5] L. F. Wei, Y.-x. Liu, and F. Nori, *Generation and control of Greenberger-Horne-Zeilinger entanglement in super-*

conducting circuits, Phys. Rev. Lett. **96**, 246803 (2006).

[6] C.-P. Yang, Q.-P. Su, S.-B. Zheng, and F. Nori, *Entangling superconducting qubits in a multi-cavity system,* New J. Phys. **18**, 013025 (2016).

[7] M. Erhard, M. Malik, M. Krenn, and A. Zeilinger, *Experimental Greenberger-Horne-Zeilinger entanglement beyond qubits,* Nat. Photon. **12**, 759 (2018).

[8] C. Song, K. Xu, H. Li, Y.-R. Zhang, X. Zhang, W. Liu, Q. Guo, Z. Wang, W. Ren, J. Hao, H. Feng, H. Fan, D. Zheng, D.-W. Wang, H. Wang, and S.-Y. Zhu, *Generation of multicomponent atomic Schrödinger cat states of up to 20 qubits,* Science **365**, 574 (2019).

[9] D. Bouwmeester, J.-W. Pan, M. Daniell, H. Weinfurter, and A. Zeilinger, *Observation of three-photon Greenberger-Horne-Zeilinger entanglement,* Phys. Rev. Lett. **82**, 1345 (1999).

[10] L. S. Bishop, L. Tornberg, D. Price, E. Ginossar, A. Nunnenkamp, A. A. Houck, J. M. Gambetta, J. Koch, G. Johansson, S. M. Girvin, and R. J. Schoelkopf, *Proposal for generating and detecting multi-qubit GHZ states in circuit QED,* New J. Phys. **11**, 073040 (2009).

[11] V. Macrì, F. Nori, and A. F. Kockum, *Simple preparation of Bell and Greenberger-Horne-Zeilinger states using ultrastrong-coupling circuit qed,* Phys. Rev. A **98**, 062327 (2018).

[12] K. Paul and A. K. Sarma, *High-fidelity entangled Bell states via shortcuts to adiabaticity,* Phys. Rev. A **94**, 052303 (2016).

[13] F. W. Strauch, K. Jacobs, and R. W. Simmonds, *Arbitrary control of entanglement between two superconducting resonators,* Phys. Rev. Lett. **105**, 050501 (2010).

[14] S. T. Merkel and F. K. Wilhelm, *Generation and detection of NOON states in superconducting circuits,* New J. Phys. **12**, 093036 (2010).

[15] J. Lee and M. S. Kim, *Entanglement teleportation via Werner states,* Phys. Rev. Lett. **84**, 4236 (2000).

[16] W. Tittel, J. Brendel, H. Zbinden, and N. Gisin, *Quantum cryptography using entangled photons in energy-time Bell states,* Phys. Rev. Lett. **84**, 4737 (2000).

[17] Y.-H. Kim, S. P. Kulik, and Y. Shih, *Quantum teleportation of a polarization state with a complete Bell state measurement,* Phys. Rev. Lett. **86**, 1370 (2001).

[18] J. P. Dowling, *Quantum optical metrology-the lowdown on high-NOON states,* Contemp. Phys. **49**, 125 (2008).

[19] M. D'Angelo, A. Garuccio, and V. Tamma, *Toward real maximally path-entangled n-photon-state sources,* Phys. Rev. A **77**, 063826 (2008).

[20] K. Kamide, Y. Ota, S. Iwamoto, and Y. Arakawa, *Method for generating a photonic NOON state with quantum dots in coupled nanocavities,* Phys. Rev. A **96**, 013853 (2017).

[21] J. Chen and L. F. Wei, *Deterministic generations of photonic NOON states in cavities via shortcuts to adiabaticity,* Phys. Rev. A **95**, 033838 (2017).

[22] D.-W. Wang, H. Cai, R.-B. Liu, and M. O. Scully, *Mesoscopic superposition states generated by synthetic spin-orbit interaction in Fock-state lattices,* Phys. Rev. Lett. **116**, 220502 (2016).

[23] M. W. Mitchell, J. S. Lundeen, and A. M. Steinberg, *Super-resolving phase measurements with a muitiphoton entangled state,* Natrue **429**, 161 (2004).

[24] L. Pezzè, A. Smerzi, M. K. Oberthaler, R. Schmied, and P. Treutlein, *Quantum metrology with nonclassical states of atomic ensembles,*

[25] A. N. Boto, P. Kok, D. S. Abrams, S. L. Braunstein, C. P. Williams, and J. P. Dowling, *Quantum interferometric optical lithography: Exploiting entanglement to beat the diffraction limit,* Phys. Rev. Lett. **85**, 2733 (2000).

[26] M. D'Angelo, M. V. Chekhova, and Y. Shih, *Two-photon diffraction and quantum lithography,* Phys. Rev. Lett. **87**, 013602 (2001).

[27] Y. Israel, S. Rosen, and Y. Silberberg, *Supersensitive polarization microscopy using NOON states of light,* Phys. Rev. Lett. **112**, 103604 (2014).

[28] J. A. Jones, S. D. Karlen, J. Fitzsimons, S. C. Ardavan, A. Benjamin, A. D. Briggs, and J. J. L. Morton, *Magnetic field sensing beyond the standard quantum limit using 10-spin NOON states,* Science **324**, 1166 (2009).

[29] I. Afek, O. Ambar, and Y. Silberberg, *High-NOON states by mixing quantum and classical light,* Science **328**, 879 (2010).

[30] D. S. Grün, L. H. Ymai, K. Wittmann W., A. P. Tonel, A. Foerster, and J. Links, *Integrable atomtronic interferometry,* Phys. Rev. Lett. **129**, 020401 (2022).

[31] D. S. Grün, K. Wittmann W., L. H. Ymai, J. Links, and A. Foerster, *Protocol designs for NOON states,* Commun. Phys. **5**, 36 (2022).

[32] J. Zhang, M. Um, D. Lv, J.-N. Zhang, L.-M. Duan, and K. Kim, *NOON states of nine quantized vibrations in two radial modes of a trapped ion,* Phys. Rev. Lett. **121**, 160502 (2018).

[33] F. Yan, S. Gustavsson, A. Kamal, J. Birenbaum, A. P. Sears, D. Hover, T. J. Gudmundsen, D. Rosenberg, G. Samach, and S. Weber, *The flux qubit revisited to enhance coherence and reproducibility,* Nat. Commun. **7**, 12964 (2015).

[34] J. Q. You, X. Hu, S. Ashhab, and F. Nori, *Low-decoherence flux qubit,* Phys. Rev. B **75**, 140515 (2007).

[35] M. J. Peterer, S. J. Bader, X. Jin, F. Yan, A. Kamal, T. J. Gudmundsen, P. J. Leek, T. P. Orlando, W. D. Oliver, and S. Gustavsson, *Coherence and decay of higher energy levels of a superconducting transmon qubit,* Phys. Rev. Lett. **114**, 010501 (2015).

[36] A. Wallraff, D. I. Schuster, A. Blais, L. Frunzio, H. R-S, J. Majer, S. Kumar, S. M. Girvin, and R. J. Schoelkopf, *Strong coupling of a single photon to a superconducting qubit using circuit quantum electrodynamics,* Nature **431**, 162 (2004).

[37] B. Peropadre, P. Forn-Díaz, E. Solano, and J. J. García-Ripoll, *Switchable ultrastrong coupling in circuit QED,* Phys. Rev. Lett. **105**, 023601 (2010).

[38] P. Forn-Díaz, L. Lamata, E. Rico, J. Kono, and E. Solano, *Ultrastrong coupling regimes of light-matter interaction,* Rev. Mod. Phys. **91**, 025005 (2019).

[39] A. F. Kockum, A. Miranowicz, S. D. Liberato, S. Savasta, and F. Nori, *Ultrastrong coupling between light and matter,* Nat. Rev. Phys. **1**, 19 (2019).

[40] T. Niemczyk, F. Deppe, H. Huebl, E. P. Menzel, F. Hocke, M. J. Schwarz, J. J. Garciaripoll, D. Zueco, T. Hömmer, and E. Solano, *Circuit quantum electrodynamics in the ultrastrong-coupling regime,* Nat. Phys. **6**, 772 (2010).

[41] J. Q. You and N. Franco, *Atomic physics and quantum optics using superconducting circuits,* Nature **474**, 589 (2011).

[42] A. Blais, A. L. Grimsmo, S. M. Girvin, and A. Wallraff, *Circuit quantum electrodynamics,*

Rev. Mod. Phys. **93**, 025005 (2021).

[43] Y.-J. Zhao, Y.-L. Liu, Y.-x. Liu, and F. Nori, *Generating nonclassical photon states via longitudinal couplings between superconducting qubits and microwave fields,* Phys. Rev. A **91**, 053820 (2015).

[44] H. Wang, M. Mariantoni, R. C. Bialczak, M. Lenander, E. Lucero, M. Neeley, A. D. O'Connell, D. Sank, M. Weides, J. Wenner, T. Yamamoto, Y. Yin, J. Zhao, J. M. Martinis, and A. N. Cleland, *Deterministic entanglement of photons in two superconducting microwave resonators,* Phys. Rev. Lett. **106**, 060401 (2011).

[45] Q. P. Su, C. P. Yang, and S. B. Zheng, *Fast and simple scheme for generating NOON states of photons in circuit qed,* Sci. Rep. **4**, 3898 (2014).

[46] S. J. Xiong, Z. Sun, J. M. Liu, T. Liu, and C. P. Yang, *Efficient scheme for generation of photonic NOON states in circuit QED,* Opt. Lett. **40**, 2221 (2015).

[47] Q.-P. Su, H.-H. Zhu, L. Yu, Y. Zhang, S.-J. Xiong, J.-M. Liu, and C.-P. Yang, *Generating double NOON states of photons in circuit QED,* Phys. Rev. A **95**, 022339 (2017).

[48] S.-f. Qi and J. Jing, *Generating NOON states in circuit QED using a multiphoton resonance in the presence of counter-rotating interactions,* Phys. Rev. A **101**, 033809 (2020).

[49] W. Wang, L. Hu, Y. Xu, K. Liu, Y. Ma, S.-B. Zheng, R. Vijay, Y. P. Song, L.-M. Duan, and L. Sun, *Converting Quasiclassical states into arbitrary Fock state superpositions in a superconducting circuit,* Phys. Rev. Lett. **118**, 223604 (2017).

[50] G.-P. Guo, H. Zhang, Y. Hu, T. Tu, and G.-C. Guo, *Dispersive coupling between the superconducting transmission line resonator and the double quantum dots,* Phys. Rev. A **78**, 020302 (2008).

[51] D. Zueco, G. M. Reuther, S. Kohler, and P. Hänggi, *Qubit-oscillator dynamics in the dispersive regime: Analytical theory beyond the rotating-wave approximation,*

[52] L. C. G. Govia and F. K. Wilhelm, *Entanglement generated by the dispersive interaction: The dressed coherent state,* Phys. Rev. A **93**, 012316 (2016).

[53] C. C. Gerry, *Preparation of multiatom entangled states through dispersive atom–cavity-field interactions,* Phys. Rev. A **53**, 2857 (1996).

[54] Q.-P. Su, T. Liu, Y. Zhang, and C.-P. Yang, *Construction of a qudit using Schrödinger cat states and generation of hybrid entanglement between a discrete-variable qudit and a continuous-variable qudit,* Phys. Rev. A **104**, 032412 (2021).

[55] X.-B. Zou, Y.-F. Xiao, S.-B. Li, Y. Yang, and G.-C. Guo, *Quantum phase gate through a dispersive atom-field interaction,* Phys. Rev. A **75**, 064301 (2007).

[56] Y. Zhang, X. Zhao, Z.-F. Zheng, L. Yu, Q.-P. Su, and C.-P. Yang, *Universal controlled-phase gate with cat-state qubits in circuit QED,* Phys. Rev. A **96**, 052317 (2017).

[57] T. Liu, B.-Q. Guo, C.-s. Yu, and W.-n. Zhang, *One-step implementation of a hybrid Fredkin gate with quantum memories and single superconducting qubit in circuit QED and its applications,* Opt. Exp. **26**, 004498 (2018).

[58] C. M. Caves, K. S. Thorne, R. W. P. Drever, V. D. Sandberg, and M. Zimmermann, *On the measurement of a weak classical force coupled to a quantum-mechanical oscillator. I. issues of principle,* Rev. Mod. Phys. **52**, 341 (1980).

[59] M. F. Bocko and R. Onofrio, *On the measurement of a weak classical force coupled to a harmonic oscillator: experimental progress,* Rev. Mod. Phys. **68**, 755 (1996).

[60] J.-s. Yan and J. Jing, *Optimizing measurement-based cooling by reinforcement learning,* Phys. Rev. A **106**, 033124 (2022).

[61] J.-s. Yan and J. Jing, *Simultaneous cooling by measuring one ancillary system,* Phys. Rev. A **105**, 052607 (2022).